Supplementary Material: Complete phase diagram of rare-earth nickelates from first-principles

Julien Varignon,[1] Mathieu N. Grisolia,[1] Jorge Íñiguez,[2] Agnès Barthélémy,[1] and Manuel Bibes[1]

[1] *Unité Mixte de Physique, CNRS, Thales, Université Paris Sud, Université Paris-Saclay, 91767, Palaiseau, France**

[2] *Materials Research and Technology Department, Luxembourg Institute of Science and Technology (LIST), 5 avenue des Hauts-Fourneaux, L-4362 Esch/Alzette, Luxembourg*

(Dated: January 15, 2017)

ENERGIES OF FERROMAGNETIC, A, C AND G-TYPE ANTIFERROMAGNETIC SOLUTIONS

Table SI I reports the energy differences between the common magnetic orderings (Ferromagnetic, A, C and G-type antiferromagnetic orders) in the orthorhombic and monoclinic phases with the monoclinic $P2_1/n$ ferromagnetic solution. We emphasize that all these antiferromagnetic states have been considered in the monoclinic $P2_1/n$ symmetry, but only the A-type AFM order could be stabilized.

	Δ E(A-AFM) ($P2_1/n$)	Δ E(FM) ($Pbnm$)	Δ E(A-AFM) ($Pbnm$)	Δ E(C-AFM) ($Pbnm$)	Δ E(G-AFM) ($Pbnm$)
Pr	220	13	439	833	996
Nd	213	35	522	1104	1307
Sm	207	58	692	1370	1438
Eu	205	51	672	1240	1288
Gd	198	54	576	1069	1110
Tb	194	49	515	977	1009
Dy	196	53	445	866	894
Y	185	55	449	878	907

TABLE I. Energy differences (in meV per 80-atom unit cell) between the Ferromagnetic, A, C and G-type antiferromagnetic orderings in the orthorhombic $Pbnm$ and $P2_1/n$ phase and the ferromagnetic solution obtained in the monoclinic $P2_1/n$ phase.

LATTICE PARAMETERS OF THE RELAXED STRUCTURES

Table SI II reports the lattice parameters of our optimized ground states.

AMPLITUDE OF DISTORTIONS

Table SI III reports the amplitude of distortions associated with each rare-earth nickelate ground state. The decomposition is performed with respect to a high symmetry cubic phase. The structure is described by two antiferrodistortive motions ($a^-a^-c^0$ and $a^0a^0c^+$ oxygen

	a (Å)	b (Å)	c (Å)	α (°)
Pr	5.306	5.403	7.551	90.102
Nd	5.327	5.350	7.543	90.074
Sm	5.395	5.255	7.478	90.052
Eu	5.425	5.209	7.440	90.015
Gd	5.447	5.169	7.401	90.047
Tb	5.453	5.139	7.376	90.096
Dy	5.463	5.117	7.340	90.119
Y	5.461	5.128	7.345	90.103

TABLE II. Lattice parameters of the relaxed ground states given in a non-conventionnal setting of the $P2_1/n$ structure.

cage rotations in Glazer's notation, R_5^- and M_2^+ irreps respectively), a breathing of the oxygen cage octahedra B_{oc} (irreps R_2^-), an antipolar motion involving the rare-earth (irreps. X_5^-), a Jahn-Teller motion (irreps. M_3^+) and an antiferroelectric motion (irreps. R_4^-).

irreps.	R_5^-	M_2^+	M_3^+	R_2^-	X_5^-	R_4^-
	$a^-a^-c^0$	$a^0a^0c^+$	Jahn-Teller	B_{oc}	-	-
Pr	1.07	0.45	0.01	0.11	0.26	0.08
Nd	1.14	0.68	0.01	0.12	0.42	0.10
Sm	1.27	0.92	0.01	0.13	0.63	0.15
Eu	1.34	1.01	0.03	0.14	0.71	0.17
Gd	1.41	1.08	0.04	0.14	0.78	0.19
Tb	1.46	1.12	0.05	0.15	0.82	0.21
Dy	1.51	1.16	0.05	0.15	0.86	0.22
Y	1.52	1.16	0.05	0.15	0.86	0.22

TABLE III. Amplitude of distortions (in Å) associated with the relaxed ground state of different nickelates.

BORN EFFECTIVE CHARGES

Tables SI IV and SI V report the Born effective charge tensors of the different nickelates in their ground state.

GROUND STATE e_g-LIKE WANNIER FUNCTIONS OF THE SMALL NI SITE

We ran additional Maximally-Localized Wannier Function optimizations in order to build the small Ni_S site e_g states in the ground state phase. To that end, we have restricted the localization procedure to the first 16 unoccupied states and we initially projected the Kohn-Sham states on two e_g states per Ni_S. As it is displayed in Figure 1, we are able to localize two e_g-like states per Ni_S, further demonstrating that these states are located in the unoccupied manifold. This observation supports the charge disproportionation scenario, although these MLWFs exhibit a certain O-2p character, which gives further evidence for the hybridization between oxygen and Ni_S states.

LEVEL OF COVALENCE

We have checked the level of covalence for a ferromagnetic solution in the monoclinic phase. For this spin arrangement, the difference of the spin-up and spin-down charge densities, integrated to the full cell, yield a magnetic moment of $2\mu_B$ per Ni_L cation. In contrast, the local magnetic moments –as estimated from integrals in Ni_L-centered spheres – yield relatively small moments of 1.17 μ_B for $PrNiO_3$ (it increases to 1.21 μ_B for $YNiO_3$). The difference between the two results comes from the hybridization of Ni-3d and O-2p orbitals, and corresponding spillage of the localized magnetic moments.

	$PrNiO_3$			$NdNiO_3$			$SmNiO_3$			$EuNiO_3$		
	x	y	z	x	y	z	x	y	z	x	y	z
x	4.20	0.22	0.02	4.15	0.30	0.05	4.12	0.40	0.10	4.12	0.42	0.13
R y	0.17	4.49	0.43	0.32	4.27	0.40	0.16	4.29	0.41	0.13	4.24	0.40
z	0.18	-0.26	3.98	0.30	-0.30	4.11	0.47	-0.25	3.88	0.54	-0.25	3.84
	x	y	z	x	y	z	x	y	z	x	y	z
x	2.35	0.21	0.00	2.21	0.20	-0.02	2.25	0.10	0.08	2.27	-0.05	-0.10
Ni_S y	-0.23	2.47	-0.38	-0.21	2.10	-0.46	-0.20	2.04	-0.14	0.17	1.95	-0.07
z	-0.19	0.52	2.14	-0.04	0.24	2.32	-0.32	0.23	1.90	0.31	0.16	1.84
	x	y	z	x	y	z	x	y	z	x	y	z
x	2.66	-0.64	-0.03	2.86	-0.85	0.01	2.49	-1.01	-0.05	2.47	1.06	0.06
Ni_L y	0.49	2.61	1.76	0.71	2.51	1.60	0.90	2.30	1.62	-0.95	2.20	1.59
z	-0.23	-1.21	2.95	-0.24	-1.37	2.51	-0.60	-1.33	2.70	0.68	-1.39	2.63
	x	y	z	x	y	z	x	y	z	x	y	z
x	-1.69	-0.11	0.01	-1.71	-0.19	0.00	-1.62	-0.28	-0.07	-1.60	-0.32	-0.10
O_1 y	-0.06	-2.10	0.08	-0.22	-1.72	0.11	-0.18	-2.07	0.12	-0.21	-2.07	0.13
z	-0.13	0.90	-3.28	-0.28	1.08	-2.95	-0.32	1.05	-2.99	-0.36	1.09	-2.90
	x	y	z	x	y	z	x	y	z	x	y	z
x	-2.34	-0.80	-0.43	-2.22	-0.87	-0.39	-1.92	0.86	-0.45	-2.00	-0.84	-0.43
O_2 y	-0.46	-2.72	-0.48	-0.40	-2.76	-0.36	0.22	-2.47	0.35	-0.24	-2.54	-0.35
z	-0.09	-0.06	-1.62	0.07	-0.08	-1.80	0.07	-0.08	-1.61	0.02	0.06	-1.62
	x	y	z	x	y	z	x	y	z	x	y	z
x	-2.68	0.54	0.54	-2.75	-0.45	-0.53	-2.83	0.21	0.72	-2.89	-0.14	-0.77
O_3 y	0.83	-2.18	-0.71	-0.94	-2.08	-0.73	0.97	-1.79	-0.90	-1.00	-1.71	-0.93
z	0.04	-0.23	-1.63	-0.17	-0.13	-1.77	-0.02	-0.30	-1.58	0.03	-0.30	-1.57

TABLE IV. Computed Born effective charges of $PrNiO_3$, $NdNiO_3$, $SmNiO_3$ and $EuNiO_3$ in the ground state.

		$GdNiO_3$			$TbNiO_3$			$DyNiO_3$			$YNiO_3$		
		x	y	z	x	y	z	x	y	z	x	y	z
O_3	x	4.11	-0.44	0.13	4.10	-0.46	0.15	4.10	0.48	-0.15	4.11	-0.44	0.13
	y	-0.14	4.23	-0.36	-0.05	4.17	-0.40	0.02	4.13	-0.40	-0.14	4.23	-0.36
	z	0.57	0.25	3.80	0.64	0.25	3.75	-0.67	0.25	3.72	0.57	0.25	3.80
		x	y	z	x	y	z	x	y	z	x	y	z
Ni_S	x	2.23	0.00	-0.12	2.26	-0.02	-0.15	2.25	0.05	0.17	2.23	0.00	-0.12
	y	-0.12	1.91	-0.01	-0.12	1.82	-0.07	0.10	1.78	-0.14	-0.12	1.91	-0.01
	z	0.30	-0.11	1.79	0.28	-0.05	1.75	-0.26	-0.02	1.73	0.30	-0.11	1.79
		x	y	z	x	y	z	x	y	z	x	y	z
Ni_L	x	2.42	-1.06	0.06	2.45	-1.12	0.06	2.43	1.13	-0.05	2.42	-1.06	0.06
	y	0.96	2.12	-1.55	1.01	2.09	-1.54	-1.02	2.05	-1.53	0.96	2.12	-1.55
	z	0.72	1.42	2.54	0.80	1.49	2.51	-0.85	1.53	2.46	0.72	1.42	2.54
		x	y	z	x	y	z	x	y	z	x	y	z
O_1	x	-1.54	0.35	-0.12	-1.57	0.37	-0.14	-1.56	-0.39	0.15	-1.54	0.35	-0.12
	y	0.20	-2.08	-0.16	0.24	-2.07	-0.14	-0.25	-2.06	-0.14	0.20	-2.08	-0.16
	z	-0.38	-1.11	-2.77	-0.41	-1.16	-2.75	0.43	-1.19	-2.69	-0.38	-1.11	-2.77
		x	y	z	x	y	z	x	y	z	x	y	z
O_2	x	-1.91	0.83	-0.44	-1.92	0.86	-0.45	-1.89	-0.86	0.45	-1.91	0.83	-0.44
	y	0.21	-2.47	0.34	0.22	-2.47	0.35	-0.22	-2.44	0.35	0.21	-2.47	0.34
	z	0.05	-0.08	-1.58	0.07	-0.08	-1.61	-0.09	-0.08	-1.60	0.05	-0.08	-1.58
		x	y	z	x	y	z	x	y	z	x	y	z
O_3	x	-2.89	-0.07	0.81	-2.97	-0.03	0.85	-2.99	0.00	-0.89	-2.89	0.07	-0.81
	y	-0.98	-1.62	0.94	-1.05	-1.59	0.99	1.07	-1.54	1.01	0.98	-1.62	0.94
	z	-0.05	0.28	-1.54	-0.06	0.27	-1.54	0.08	0.26	-1.52	0.06	0.28	-1.52

TABLE V. Computed Born effective charges of $GdNiO_3$, $TbNiO_3$, $DyNiO_3$ and $YNiO_3$ in the ground state.

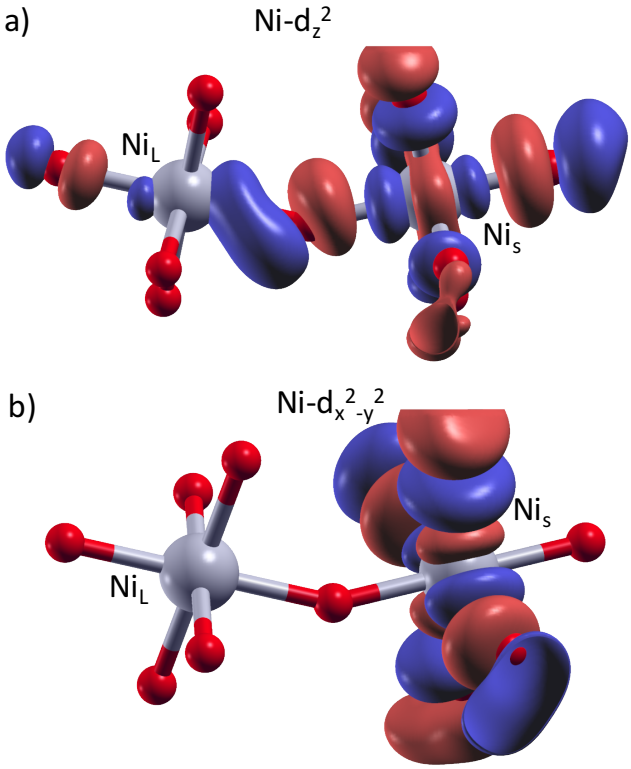

FIG. 1. e_g **states of the small Ni site** (a) d_z^2 states obtained in both spin channel on a small Ni site by restricting the localization procedure to the 16 first unoccupied states.(a) $d_x z^2 - y^2$ states obtained in both spin channel on a small Ni site by restricting the localization procedure to the 16 first unoccupied states.

NON COLLINEAR CALCULATIONS

We have performed additional geometry optimizations on $SmNiO_3$ allowing the spin-orbit interaction and non collinear spin arrangements. We have considered all the magnetic states discussed in the main manuscript (ferromagnetic and complex E, S and T-type antiferromagnetic orderings) with spins initially aligned along the three possible crystallographic axes (labeled as X, Y and Z). We emphasize that for computational cost reasons, the K-point mesh has been downgraded to 4×2×2 k-points. Spin-spirals proposed in references (42) (Spiral-1) and (5) (Spiral-2) of the main manuscript were also tested. We have also tried $\uparrow\rightarrow\downarrow\leftarrow$ spin chains in the (ab)-plane with different stacking along the $\vec{c}$ axis and spin orientations. However, these magnetic states are found to relax toward a S-type antiferromagnetic state with a $\uparrow 0 \downarrow 0$ chains and are not presented.

Energy differences and the computed magnetic moments on both Ni sites are summarized in table VI. The inclusion of the spin-orbit interaction does not change the key results of the main manuscript, *i.e.* the complex antiferromagnetic orderings remain more stable than the ferromagnetic solution and the two Ni sites still resemble to a low spin Ni_S^{4+} and a Ni_L^{2+} configuration. We emphasize that a full inspection of the J parameter has not been performed and that we have kept an effective U approach with $U_{\rm eff}$= 2 eV on Ni 3d states.

	ΔE (meV)	Ni_S magnetic moment (μ_B)				Ni_L magnetic moment (μ_B)			
		μ^x	μ^y	μ^z	$\|\|\mu\|\|$	μ^x	μ^y	μ^z	$\|\|\mu\|\|$
Pbnm-FM-X	97.85	0.88	-0.04	-0.04	0.88	0.88	0.04	0.04	0.88
Pbnm-FM-Y	99.70	0.05	0.87	0.01	0.87	-0.05	0.89	0.01	0.89
Pbnm-FM-Z	99.47	0.03	0.04	0.88	0.88	-0.04	-0.01	0.88	0.88
FM-X	0.00	0.53	0.03	-0.01	0.53	1.21	0.08	0.02	1.21
FM-Y	-1.12	-0.03	0.52	-0.01	0.53	-0.08	1.20	-0.12	1.21
FM-Z	-0.05	0.01	0.02	0.52	0.52	-0.02	0.14	1.20	1.21
AFME-X	-33.77	0.17	0.04	0.00	0.18	1.20	-0.26	-0.04	1.23
AFME-Y	-32.17	-0.08	0.14	-0.08	0.18	0.49	0.87	-0.71	1.23
AFME-Z	-33.73	-0.01	0.06	0.16	0.18	0.11	0.55	1.09	1.23
AFMS-X	-158.91	0.00	0.00	0.00	0.00	1.13	-0.43	-0.10	1.21
AFMS-Y	-158.00	0.00	0.00	0.00	0.00	0.29	1.10	-0.44	1.22
AFMS-Z	-158.19	0.00	0.00	0.00	0.00	0.12	0.37	1.15	1.22
AFMT-X	-162.00	0.00	0.00	0.00	0.00	-1.16	0.37	-0.06	1.22
AFMT-Y	-162.76	0.00	0.00	0.00	0.00	-0.26	-1.12	0.39	1.22
AFMT-Z	-162.22	0.00	0.00	0.00	0.00	-0.04	-0.43	-1.14	1.22
Spiral-1	-158.96	0.00	0.00	0.00	0.00	0.09	0.89	0.82	1.22
Spiral-2	-158.96	0.00	0.00	0.00	0.00	0.32	1.11	0.38	1.22

TABLE VI. Energy difference (in meV per 80-atom unit cell) between the different magnetic states and initial spin directions. The energy reference is set to the monoclinic ferromagnetic solution with the spins aligned along the X direction. The projected spin components and the global magnetic moments (in μ_B) on both Ni_S and Ni_L sites are also reported.